Available online at www.sciencedirect.com
SCIENCE DIRECT®
European Journal of Mechanics B/Fluids 24 (2005) 366–378

Fluid mixing induced by vibrating walls

Fredrik Carlsson [a,1], Mihir Sen [b], Lennart Löfdahl [a,*]

[a] *Department of Thermo and Fluid Dynamics, Chalmers University of Technology, 41296 Gothenburg, Sweden*
[b] *Department of Aerospace and Mechanical Engineering, University of Notre Dame, Notre Dame, IN 46556, USA*

Received 14 October 2003; received in revised form 27 September 2004; accepted 7 October 2004

Available online 22 December 2004

Abstract

Recent progress in micro-fluid dynamics has identified an increased demand for efficient mixing of highly viscous fluids in small channels and cavities. One way to do this is through the steady streaming generated by the vibration of solid boundaries. In this paper we investigate the mixing properties of such streaming flows in an infinite channel. A Newtonian fluid is confined within flexible walls with transverse motion in the form of standing waves of small amplitude. The velocity field is determined using a perturbation approach with the slope of the wall as a small parameter [Phys. Fluids 16 (2004) 1822]. Streaming occurs at second order with the formation of cellular flow patterns in the channel. The Lagrangian velocities were found to mimic the Eulerian except for flows at large channel half-widths and low frequencies. Most effective mixing is observed for flows at channel half-widths of similar, or lower, order than the vibratory wavelength and for sufficiently high frequencies.

Keywords: Mixing; Streaming; Unsteady; Waves; Vibrating

1. Introduction

This paper presents a study of the mixing properties of flows generated by the transverse vibration of a solid wall. Though the time-averaged velocity of the moving wall is inherently zero, nonlinear interactions of the unsteady flow with itself engender a time-independent flow that is added to the unsteady part. This intriguing feature that a fluctuating flow results in a nonzero mean is denoted steady streaming [2,3]. The present analysis is primarily motivated by the ability of such streaming motions to enhance mixing in highly viscous fluids, where the intense mixing due to turbulent motions is not possible.

The appearance of streaming motion forced by unsteady boundaries depends on the spatial and temporal behavior of the specific boundary. Steady streaming induced by oscillatory flows over wavy surfaces was studied by Lyne [4]. Lyne assumed small amplitudes of the wavy surface in comparison to the viscous boundary layer formed over the vibrating wall. Investigating the time average of the fluctuating flow, he found streaming in cellular flow patterns. An attempt to extend his analysis was undertaken by Kaneko and Honji [5] who, by considering higher order terms, provided further details on the cellular flow complemented by experimental evidence of its existence. More recently, steady streaming induced by a randomly vibrating wavy wall was examined in a micro-gravity environment by Volfson and Vinals [6].

* Corresponding author.
E-mail address: lelo@tfd.chalmers.se (L. Löfdahl).
[1] Currently at Fluent Sweden AB, Vestagatan 2A, 416 64 Gothenburg, Sweden.

0997-7546/$ – see front matter
doi:10.1016/j.euromechflu.2004.10.006

A surface experiencing an oscillatory motion in the form of a travelling wave gives rise to streaming parallel to the surface. Thus, in contrast to the vibration of wavy walls, travelling waves generate a steady flow in a preferred direction, generally in the direction of the wave. This pumping effect is denoted peristaltic pumping. Several studies on peristaltic transport have been conducted over the years and analytical solutions have been obtained for two-dimensional or axisymmetric flows in infinite tubes, for either small amplitudes and arbitrary Reynolds number, or arbitrary amplitudes with small wall slopes and insignificant inertia. Early studies on this subject are reviewed in Jaffrin and Shapiro [7]. More recent investigations were performed using lubrication theory by Hung and Brown [8], Pozrikidis [9] and Li and Brasseur [10], the last generalizing the analysis to arbitrary wave shapes and finite-length tubes. A few investigations have reported numerical results where the restriction of a small parameter is relaxed [11,12]. Research on peristaltic flows has received justification foremost in medical applications, such as peristaltic pumping in the ureter, but also in engineering, e.g. transport of fluids where conventional pumping is considered inappropriate.

Recent development of micro-electro-mechanical systems (MEMS) has enabled constructions of tiny fluid mechanical devices used, for example, for the mixing of reagents and chemicals in small-scale experiments. Simple methods of producing fluid motions thus are a necessity for successful miniature devices. At small scales viscous effects commonly are important and conventional techniques of mixing and transporting fluids often are ineffective and complicated to use. The lack of effective methods to mix and transport viscous fluids has led to research in this area [13–18]. Encouraged by the need for efficient mixing of flows in small devices, Selverov and Stone [19] and Yi et al. [20] examined the streaming flow generated by small amplitude travelling waves propagating along the boundaries of closed rectangular cavities. The former primarily focused on high-frequency flows and the latter extended their analysis numerically to incorporate large amplitude waves. In these studies the fluid motion is peristaltically driven; the end walls, however, serve to restrict the flow and thus force a cellular flow pattern that is necessary in order to effectively mix the fluid.

Carlsson et al. [1] extended the works by Selverov and Stone [19] and Yi et al. [20] by considering steady streaming in a two-dimensional channel generated by small amplitude vibrations in the form of standing waves. Streaming in cellular flow patterns was observed. No peristaltic pumping is generated by standing waves, instead the cellular flow was similar to the findings in Lyne [4] and Kaneko and Honji [5]. Standing waves by themselves produce circulatory streaming motions that can be used to mix fluids. In this paper we investigate the ability of the cellular flows found in Carlsson et al. [1] to enhance mixing in highly viscous fluids.

A theoretical analysis employing perturbation methods is performed to investigate the mean Lagrangian velocity of specific fluid particles. A Newtonian fluid confined in a two-dimensional infinitely-long channel in which the solid walls vibrate transversely as standing waves is considered. The slope of the vibrating wall is assumed small and accordingly used as a perturbation parameter. Analytical expressions of the Eulerian velocity field are obtained from Carlsson et al. [1]. These are used to establish the time-averaged second-order Lagrangian velocities for a range of channel half-widths and frequencies. Next, Poincaré sections are constructed numerically in order to demonstrate the type of mixing in the channel. Finally, a large number of particles are marked and followed in time to illustrate the capacity of the steady streaming to deform a material region within the fluid. Many of the calculations below were made using Mathematica and some of the lengthy expressions are not explicitly shown in the interests of space.

2. Mathematical formulation

Consider a two-dimensional infinitely-long channel with its boundaries located at $\pm y_w$, where the region $-y_w < y < y_w$ is occupied by an incompressible Newtonian viscous fluid. To allow the solid boundaries to vibrate transversely in the form of a standing wave, the wall coordinate is set to

$$y_w = h + \frac{\epsilon}{k}\cos kx \cos \omega t, \tag{1}$$

where $k = 2\pi/\lambda$ is the wavenumber, λ is wavelength of the wavy surface, $\omega = 2\pi f$ is the radian frequency, and f is the frequency of vibration. The dimensionless parameter ϵ is the slope of the wall, that is $\epsilon = ak$, where a is the amplitude of vibration. In Fig. 1 a sketch of the wall displacement is shown. The flow driven by the wall motion is periodic in x as well as symmetric with respect to the channel centreline.

Since the wall motion is only in the vertical direction, it means the wall is extensible or that the deformation is linear. The latter is a valid approximation if the vibrations occur with small slopes, i.e. with $\epsilon \ll 1$. This will be the focus of the present investigation.

If velocities are scaled with $\epsilon\omega/k$, lengths with k and time with ω^{-1}, we get the dimensionless parameters

$$\epsilon = ak, \quad H = hk, \quad \text{and} \quad \alpha^2 = \frac{\omega}{\nu k^2}. \tag{2}$$

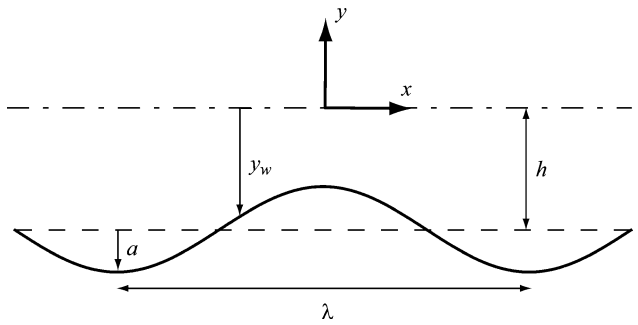

Fig. 1. Sketch of vibrating wall.

These parameters represent the slope of the surface, the channel half-width, and the wall frequency (or a Reynolds number), respectively.

The position of the wall boundary is highly time dependent which must be taken into account. For this reason the time-dependent position of the surface is dealt with here by transforming the coordinate system so that it follows the motion of the wall. Accordingly the new coordinates are

$$\xi = x, \quad \eta = y\frac{H}{H + \epsilon\cos x\cos t} \quad \text{and} \quad \tau = t, \tag{3}$$

i.e. the y coordinate is compressed by the transverse wall motion. The new coordinate system is non-orthogonal and time-dependent.

Using (3) we obtain an equation governing the flow bounded by the vibrating surfaces

$$\partial_\tau \Delta_{tc}\psi + \epsilon(\partial_\eta\psi\partial_\xi\Delta_{tc}\psi - \partial_\xi\psi\partial_\eta\Delta_{tc}\psi) - \alpha^{-2}\Delta_{tc}^2\psi = P(\xi,\eta,\tau), \tag{4}$$

where ψ represents the stream function and $\Delta_{tc} = \partial_\xi^2 + \partial_\eta^2$. $P(\xi,\eta,\tau)$, which is a lengthy expression and not given here, plays the role of a source term taking care of accelerations and the non-orthogonality inherent in the new coordinate system.

Fluid particles located on the surface must obey the no-slip condition, so that at the wall

$$\partial_\eta\psi(\xi,\eta = H,\tau) = 0, \qquad \partial_\xi\psi(\xi,\eta = H,\tau) = \cos\xi\sin\tau. \tag{5}$$

At the channel centre we have

$$\partial_\eta^2\psi(\xi,\eta = 0,\tau) = 0, \qquad \partial_\xi\psi(\xi,\eta = 0,\tau) = 0. \tag{6}$$

3. Flow field

Carlsson et al. [1] constructed a perturbation solution for the flow in the vibrating channel. In that analysis equation (4) together with (5) and (6) were perturbed using ϵ as the parameter, and the first-order and time-averaged second-order equations were solved.

3.1. First-order solution

At first order the flow is oscillatory in nature and is described by the following equation

$$\psi_0(\eta) = \mathrm{i}\frac{-A\cosh AH\sinh\eta + \cosh H\sinh A\eta}{-A\cosh AH\sinh H + \cosh H\sinh AH}\sin\xi\ \mathrm{e}^{-\mathrm{i}\tau} + \text{c.c.}, \tag{7}$$

where the index 0 denotes a first-order solution, $A = \sqrt{1 - \mathrm{i}\alpha^2}$, and c.c. is the complex conjugate.

At the wall the no-slip condition gives rise to an oscillatory boundary layer formed by the outwards diffusion of vorticity. The extent of that boundary layer is proportional to $\delta_\nu = \sqrt{\nu/\omega}$, commonly referred to as the Stokes-layer thickness, which in this problem is contained in the term $A\eta$. Another significant length scale is the wavelength λ which governs the exponential decay in the inviscid solution to the problem. The character of the solution thus strongly depends on α relating the viscous and inviscid scales, and the parameter H which may put a geometrical restriction onto the oscillatory flow through the symmetry condition at the centre of the channel.

3.2. Second-order solution

Non-linear interactions of first-order quantities induce steady streaming at second order [2]. The solution governing the streaming in the channel is

$$\begin{aligned}\psi_1^{(s)}(\xi,\eta) = \sin(2\xi)\big[&a_1\eta\cosh 2\eta + a_2\sinh 2\eta + a_3\cosh\eta + a_4\sinh\eta + a_5\cos\gamma\eta\ \sinh\beta\eta + a_6\sin\gamma\eta\ \cosh\beta\eta\\ &+ a_7\eta\sin\gamma\eta\ \sinh\beta\eta + a_8\eta\cos\gamma\eta\ \cosh\beta\eta + a_9\sin 2\gamma\eta + a_{10}\sinh 2\beta\eta + a_{11}\cos\gamma\eta\ \sinh(1+\beta)\eta\\ &+ a_{12}\sin\gamma\eta\ \cosh(1+\beta)\eta + a_{13}\cos\gamma\eta\ \sinh(1-\beta)\eta + a_{14}\sin\gamma\eta\ \cosh(1-\beta)\eta\big],\end{aligned} \tag{8}$$

where $\beta = \sqrt{R}\cos\theta$, $\gamma = \sqrt{R}\sin\theta$, $R = (1+\alpha^4)^{1/4}$ and $\theta = 1/2\arctan(-\alpha^2)$. The coefficients a_1 to a_{14} depend on α and H and are not given here since they are extremely lengthy.

Note that all the figures containing information obtained from $\psi_1^{(s)}(\xi,\eta)$ are shown in the fixed coordinate system (x, y). The time dependence of η enters the problem at third order when transforming $\psi_1^{(s)}(\xi,\eta)$ into the fixed system (x, y).

3.3. Streaming

The symmetry and periodicity of the problem prohibit any bulk flow in the channel, i.e. the moving walls do not generate a net pressure gradient in the channel. The streamlines form closed loops creating a cellular flow pattern.

Increasing the channel half-width means that H becomes less important for the flow since the extent of the flow in the y direction is determined by the larger of λ and δ_ν, the latter being the larger only for small values of α^2. In the extreme case we let H go to infinity and the solution tends to that of standing waves operating on a surface in a semi-infinite domain.

Varying α^2 for $H \gg 1$ shows three regions of distinctly different flow patterns. If α^2 is small, the flow is highly viscous and the flow structures are primarily determined by viscous diffusion. Fig. 2(a) displays velocity profiles obtained for $\alpha^2 = 2$ and $H = 50$. These profiles give rise to circulatory flow cells in two layers over the wall, shown using streamlines in Fig. 3(a). Increasing α reveals that the outer cells suppress the near-wall cells which eventually disappear and only one layer of cells exists as in Figs. 2(b) and 3(b) which show velocity profiles and flow cells at $\alpha^2 = 50$ and $H = 50$. At an α^2 of approximately 90 another change in flow pattern is observed. The single layer of cells is stretched until each cell simultaneously breaks down into three new cells separating the flow into viscous, intermediate and inviscid regions. Figs. 2(c) and 3(c) show the flow at $\alpha^2 = 150$ and $H = 50$ with these three regions. The characteristic amplitude of the velocity, or strength of the cell, is at first largest for

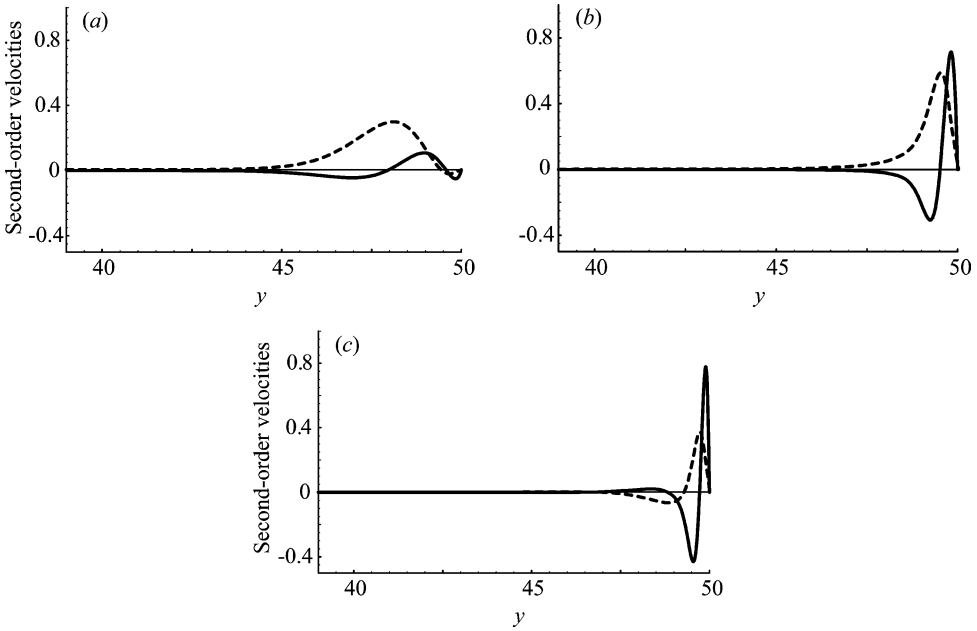

Fig. 2. Time-averaged second-order velocity profiles as a function of wall-normal distance. Solid lines are $u_1^{(s)}(\xi,\eta)$, dashed lines are $v_1^{(s)}(\xi,\eta)$. Profiles are at $x = 2\pi/3$ and $H = 50$. (a) $\alpha^2 = 2$; (b) $\alpha^2 = 50$; (c) $\alpha^2 = 150$. Only a fraction of the channel is shown. $y = H$ is at vibrating wall.

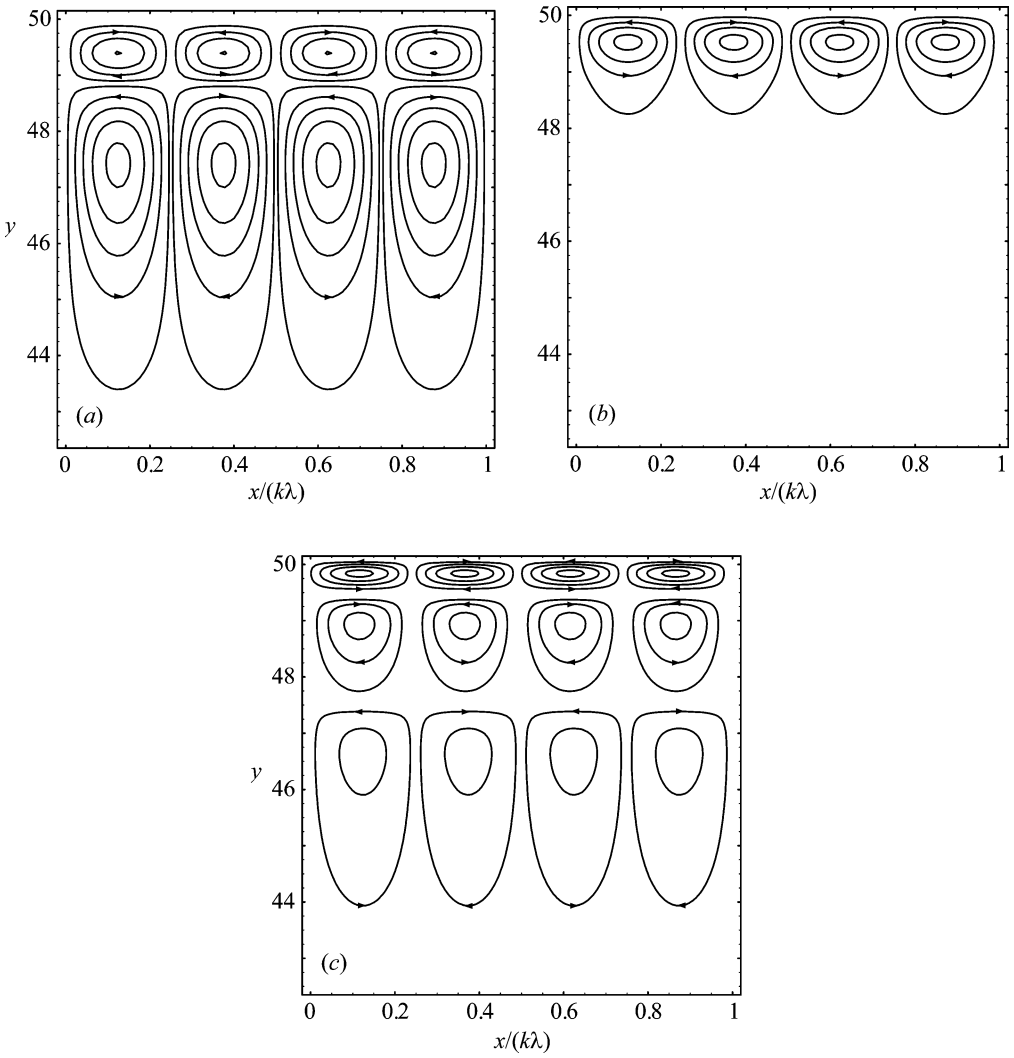

Fig. 3. Streamlines showing time-averaged second-order flow field for $H = 50$. (a) $\alpha^2 = 2$; (b) $\alpha^2 = 50$; (c) $\alpha^2 = 150$. Only a fraction of channel is shown. $y = H$ is at vibrating wall.

the cells adjacent to the wall and least for the outermost cell layer. Note that the latter is hardly observable in Fig. 2(c). With a further increase of α^2 the cells in the viscous region tend to move toward the wall and become insignificant in size and strength compared to the intermediate cells. The outer cell layer remains weak and the flow at high values of α^2 is primarily dominated by one cell layer similar to that in Fig. 3(b).

As H is diminished its impact on the streaming flow increases. By setting H to unity the surface wavelength is comparable in size to the channel half-width. The flow depends on the vibration of both channel walls regardless of α^2 since the inviscid part of the solution scales with λ. Varying α^2 reveals two distinct flow regions in comparison to the three found for $H \gg 1$.

At small α^2 only one layer of cells is formed. Fig. 4(a) displays the velocity profiles obtained at an α^2 of 10. The flow generated occupies the whole channel and the centre of the cells are located in the middle of the half channel, as shown in Fig. 5(a). By increasing α^2 there is a reduction in size of the existing flow cells together with a motion of their centre of rotation towards the wall that is evident in Figs. 4(b) and 5(b). At an α^2 of approximately 110 the flow changes character by the formation of another cell layer in the outer region; the new cellular structure is shown in Figs. 4(c) and 5(c).

A more complete picture of where in parameter space the different flow regions occur is obtained by finding critical values of α^2 for all H. If a critical value is defined as being the α^2 at which a new layer of flow cells is formed or destroyed, the different flow regions are clearly distinguished by critical lines in a parameter plot, Fig. 6.

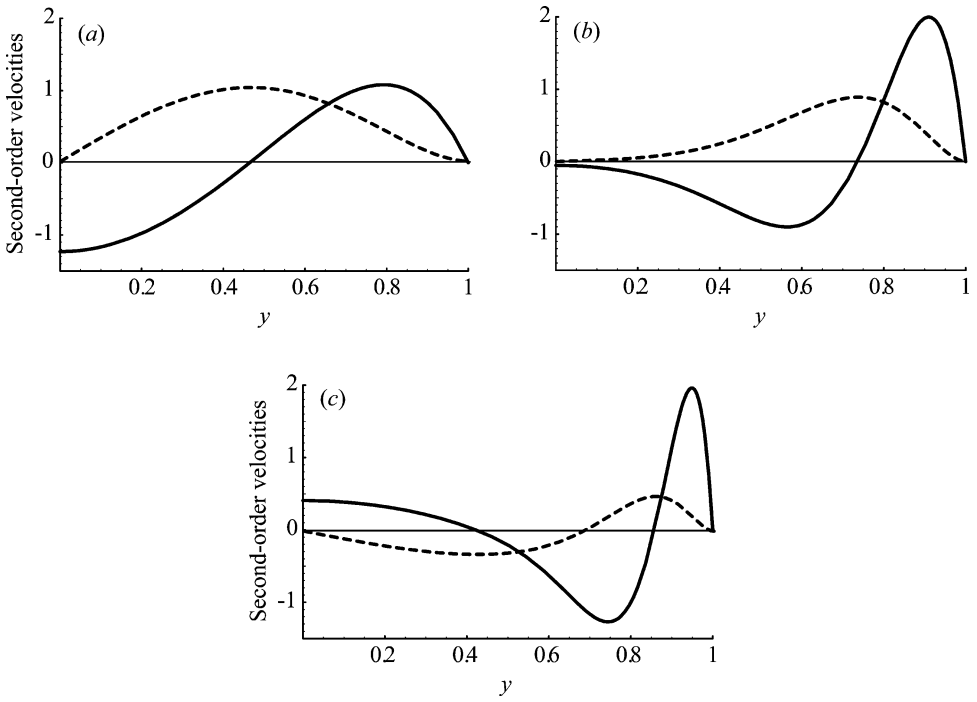

Fig. 4. Time-averaged second-order velocity profiles as a function of wall-normal distance. Solid lines are $u_1^{(s)}(\xi,\eta)$ and dashed lines are $v_1^{(s)}(\xi,\eta)$. Profiles are given at $x = 2\pi/3$ and $H = 1$. (a) $\alpha^2 = 10$; (b) $\alpha^2 = 100$; (c) $\alpha^2 = 300$. $y = H$ is at vibrating wall.

4. Mixing due to vibrating walls

Mixing of passive scalars in a quiescent fluid is solely an effect of molecular diffusion. The effectiveness of this depends on the mass and heat diffusion coefficients for mass and heat transfer problems, respectively. If the fluid begins to flow, momentum transfer within the fluid enhances mixing, an effect denoted advective mixing. The impact of advective mixing in comparison to molecular diffusion is governed by the Peclet number $Pe = \alpha^2 Sc$, where the Schmidt number $Sc = \nu/D$, D being the diffusion coefficient. For heat-transfer D is replaced by the thermal diffusivity and Sc by the Prandtl number, Pr. In viscous fluids, Sc and Pr are commonly of order one or substantially higher and thus, for a fluid in motion, the advective transport generally dominates mixing, especially for increasing α^2.

In order to examine mixing induced by vibrating surfaces we assume that Sc or Pr is large and in the analysis we let them become infinite, so that transport of passive scalars will be demonstrated by constructing fluid particle paths.

4.1. Averaged Lagrangian velocities

To shed light on how the flow transports passive scalars and how this mixing is related to the Eulerian velocity field we employ a Lagrangian description of the flow field. For each individual fluid particle the time average of its velocity is calculated. The present analysis is similar to that of Selverov and Stone [19] for the peristaltically driven flow in a confined rectangular channel, and is also commonly adopted in many water-wave problems.

If $\mathbf{X}(t) = (X(t), Y(t))$ is the position of a fluid particle, the Eulerian velocity field is described by

$$\frac{\mathrm{d}\mathbf{X}(t)}{\mathrm{d}t} = \epsilon \mathbf{u}\big(\mathbf{X}(t), t\big). \tag{9}$$

Given the initial conditions, $\mathbf{X}(0) = \mathbf{X}_0 = (X_0, Y_0)$, the paths of each individual fluid particle are obtained by solving this equation.

We can expand the position and Lagrangian velocity of a particle in power series of ϵ as

$$\mathbf{X}(t) = \mathbf{X}_0 + \epsilon \mathbf{X}_1(t) + \epsilon^2 \mathbf{X}_2(t) + \cdots \tag{10}$$

and

$$\mathbf{u}^L(t) = \epsilon \mathbf{u}_1^L(t) + \epsilon^2 \mathbf{u}_2^L(t) + \cdots. \tag{11}$$

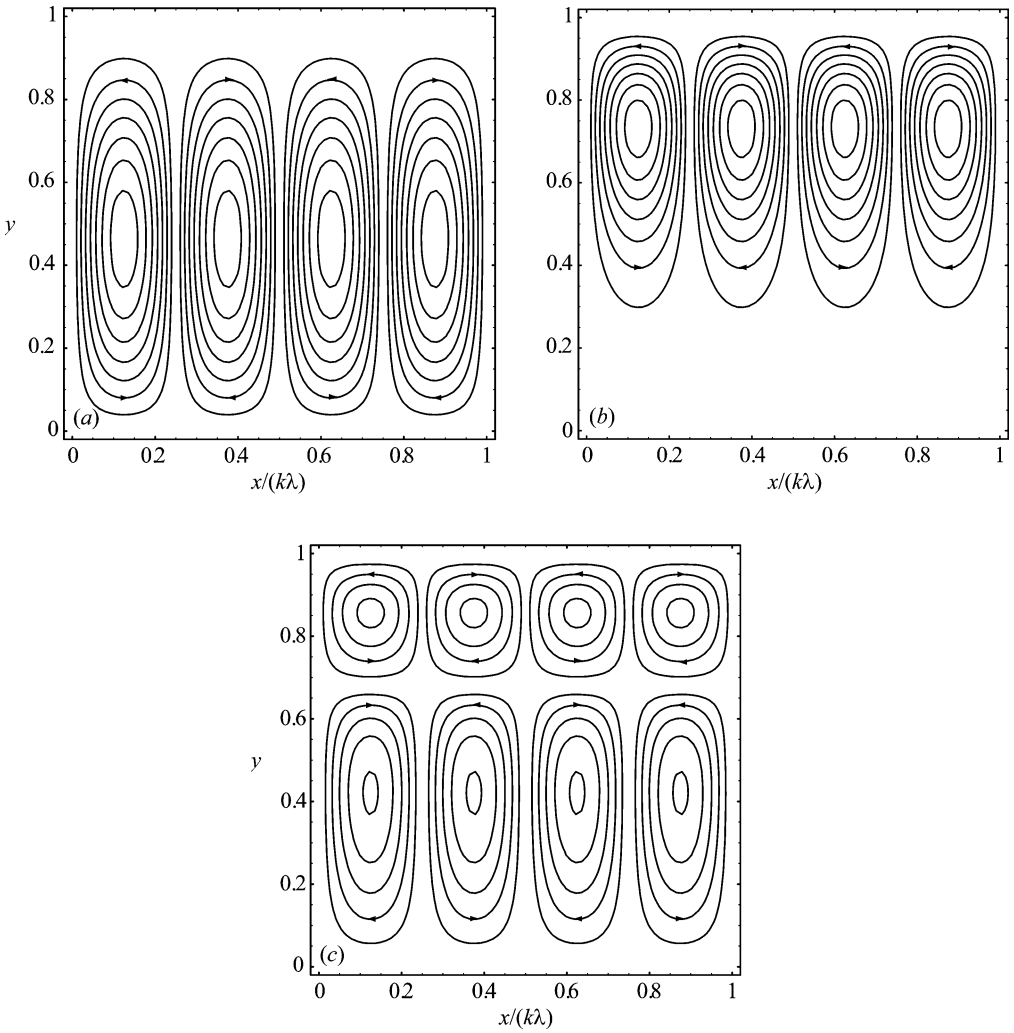

Fig. 5. Streamlines showing the time-averaged second-order flow field for $H = 1$. (a) $\alpha^2 = 2$; (b) $\alpha^2 = 100$; (c) $\alpha^2 = 300$. $y = H$ is at vibrating wall.

It is evident that $|\mathbf{X} - \mathbf{X}_0|$ is of order ϵ during one period of the oscillation. The Eulerian velocity, $\mathbf{u}(\mathbf{X}(t), t)$, can therefore be expanded in a Taylor series around the initial condition $\mathbf{X}_0$ to give

$$\mathbf{u}\big(\mathbf{X}(t), t\big) = \mathbf{u}(\mathbf{X}_0, t) + (\mathbf{X} - \mathbf{X}_0) \cdot \nabla \mathbf{u}(\mathbf{X}_0, t) + \cdots. \tag{12}$$

In the viscous region, i.e. in the vicinity of the vibrating wall, velocity gradients are of order α. Eq. (12) demands that $\epsilon\alpha \ll 1$ in these regions in order to describe the behavior of the Eulerian velocity correctly. Farther out from the wall it is, however, sufficient that $\epsilon \ll 1$. If the Eulerian perturbation expansion of ψ [1] is substituted into the definition of ψ, namely $\mathbf{u} = (\partial_y \psi, -\partial_x \psi)$, the resulting velocity perturbation can be combined with (12) to give

$$\mathbf{u}\big(\mathbf{X}(t), t\big) = \mathbf{u}_0(\mathbf{X}_0, t) + \epsilon \mathbf{u}_1(\mathbf{X}_0, t) + \mathbf{X}_1 \cdot \nabla \mathbf{u}_0(\mathbf{X}_0, t) + \cdots. \tag{13}$$

Finally, to obtain a perturbation expansion of the Lagrangian velocity, Eq. (13) is substituted into (9) and the resulting problem is investigated order by order in ϵ.

The Lagrangian velocity at leading order is described by

$$u_1^L(t) = \frac{\mathrm{d}X_1}{\mathrm{d}t} = u_0(X_0, Y_0, t), \tag{14}$$

$$v_1^L(t) = \frac{\mathrm{d}Y_1}{\mathrm{d}t} = v_0(X_0, Y_0, t). \tag{15}$$

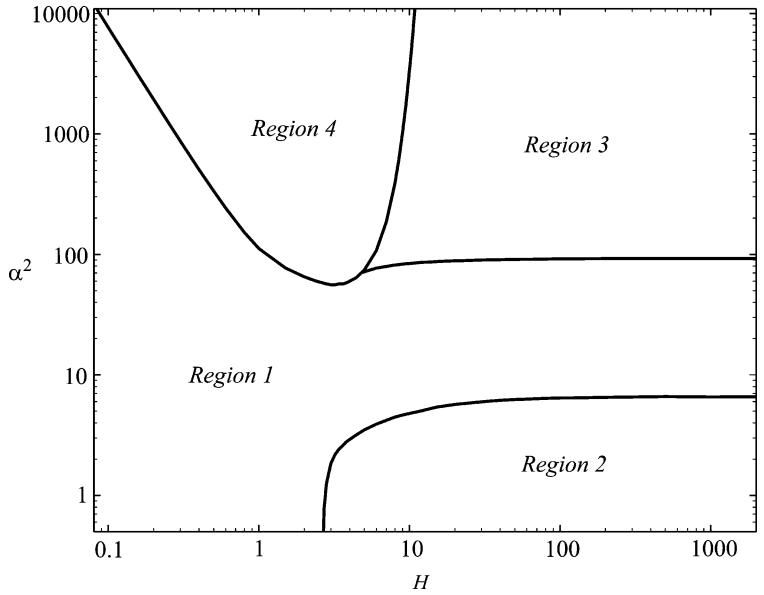

Fig. 6. α^2 as a function of H. Solid lines are critical values of α^2. The four regions represent different types of cellular flows in channel: cells in single layer in region 1 (Fig. 5(a), two layers of cells in region 2 (Fig. 3(a)), three-cell layers in region 3 (Fig. 3(c)), and two layers of cells in region 4 (Fig. 5(c)).

The first-order velocities on the right-hand sides of (14) are obtained from (7). These velocities are periodic functions of t with zero mean so that the time average over a period of the Lagrangian velocity is zero, i.e.

$$\langle \mathbf{u}_1^L \rangle = \mathbf{0}. \tag{16}$$

The fluid particles thus follow closed orbits at leading order for all possible initial conditions. The particle paths describing these orbits are obtained by integrating Eq. (14) as

$$X_1(t) = X_0 + \sin X_0 \big[F_{X1}(Y_0) \sin t + F_{X2}(Y_0)(\cos t - 1) \big], \tag{17}$$

$$Y_1(t) = Y_0 + \cos X_0 \big[F_{Y1}(Y_0) \sin t + F_{Y2}(Y_0)(\cos t - 1) \big], \tag{18}$$

where

$$F_{X1} = a_{X1} \cos \gamma Y_0 \ \cosh \beta Y_0 + b_{X1} \sin \gamma Y_0 \ \sinh \beta Y_0 + c_{X1} \cosh Y_0, \tag{19}$$

$$F_{X2} = a_{X2} \cos \gamma Y_0 \ \cosh \beta Y_0 + b_{X2} \sin \gamma Y_0 \ \sinh \beta Y_0 + c_{X2} \cosh Y_0, \tag{20}$$

$$F_{Y1} = a_{Y1} \sin \gamma Y_0 \ \cosh \beta Y_0 + b_{Y1} \cos \gamma Y_0 \ \sinh \beta Y_0 + c_{Y1} \sinh Y_0, \tag{21}$$

$$F_{Y2} = a_{Y2} \sin \gamma Y_0 \cosh \beta Y_0 + b_{Y2} \cos \gamma Y_0 \ \sinh \beta Y_0 + c_{Y2} \sinh Y_0. \tag{22}$$

The coefficients $a_{X1}, \ldots, c_{Y2}$ are not given here.

In order to observe the net transport of fluid particles the second order Lagrangian problem needs to be considered, that is

$$u_2^L(t) = u_1(X_0, Y_0, t) + X_1(t) \frac{\partial u_0}{\partial x}(X_0, Y_0, t) + Y_1(t) \frac{\partial u_0}{\partial y}(X_0, Y_0, t), \tag{23}$$

$$v_2^L(t) = v_1(X_0, Y_0, t) + X_1(t) \frac{\partial v_0}{\partial x}(X_0, Y_0, t) + Y_1(t) \frac{\partial v_0}{\partial y}(X_0, Y_0, t). \tag{24}$$

The mean drift of a particle starting at position $\mathbf{X}_0$ is computed by taking the time average of (23) over a period to yield

$$\big\langle u_2^L(t) \big\rangle = \big\langle u_1(X_0, Y_0, t) \big\rangle + \left\langle X_1(t) \frac{\partial u_0}{\partial x}(X_0, Y_0, t) \right\rangle + \left\langle Y_1(t) \frac{\partial u_0}{\partial y}(X_0, Y_0, t) \right\rangle, \tag{25}$$

$$\big\langle v_2^L(t) \big\rangle = \big\langle v_1(X_0, Y_0, t) \big\rangle + \left\langle X_1(t) \frac{\partial v_0}{\partial x}(X_0, Y_0, t) \right\rangle + \left\langle Y_1(t) \frac{\partial v_0}{\partial y}(X_0, Y_0, t) \right\rangle, \tag{26}$$

where the time average of u_1 and v_1 are obtained from Eq. (8). The final lengthy expressions for the mean Lagrangian velocities are not presented here.

The mean Lagrangian velocity is the averaged velocity of individual particles in the flow in contrast to the mean Eulerian velocity which provides the average velocity of all particles passing a specified fixed point in space. These two velocities may differ substantially depending on the flow under consideration. Fig. 7 displays mean Lagrangian velocity profiles, obtained at large H, as a function of the wall-normal initial position Y_0. Note that adjacent to the vibrating wall the Lagrangian velocities do not correctly represent the net transport of particles, an effect caused by the Taylor series expansion of the Eulerian velocity around $\mathbf{X}_0$. The corresponding Eulerian velocities are shown in Fig. 2. For small α^2, i.e. for flows in region 2 of Fig. 6, the Eulerian mean velocity differs qualitatively in shape from the Lagrangian velocity obtained at the same α^2, as is obvious on comparing Figs. 2(a) and 7(a). In the vicinity of the wall the Lagrangian and Eulerian velocity are opposite to each other. On increasing α^2, however, the Lagrangian velocity profiles qualitatively resemblance the Eulerian profiles, as seen by comparing Figs. 7(b), (c) and 2(b), (c).

Mean Lagrangian velocity profiles obtained for $H = 1$ are shown in Fig. 8 and these profiles resemblance the mean Eulerian velocity for all values of α^2; see Fig. 4. Thus, in regions 1, 3 and 4 of Fig. 6 the steady Eulerian velocity in a specified point is a qualitative estimator for the net velocity, during one period of oscillation, of a particle starting in this point. Selverov and Stone [19] observed an equivalent similarity between mean Lagrangian and Eulerian velocities in their peristaltic mixer. They also found a disagreement in the velocities at low frequencies, similar to our findings of the flow in region 2.

4.2. Advection of passive tracers

The Lagrangian mean velocity of a specified particle indicates the average rate at which that particle is displaced, but provides no information on the spatial distribution of the net displacement. To obtain this information, Eq. (9) is solved numerically using the analytical expression for the Eulerian velocity. In the present analysis the time-dependent part of the second-order velocity is not computed. This term, however, contributes to the net displacement at order ϵ^3. Thus, the net displacement of particles is correct to second order during one period of oscillation.

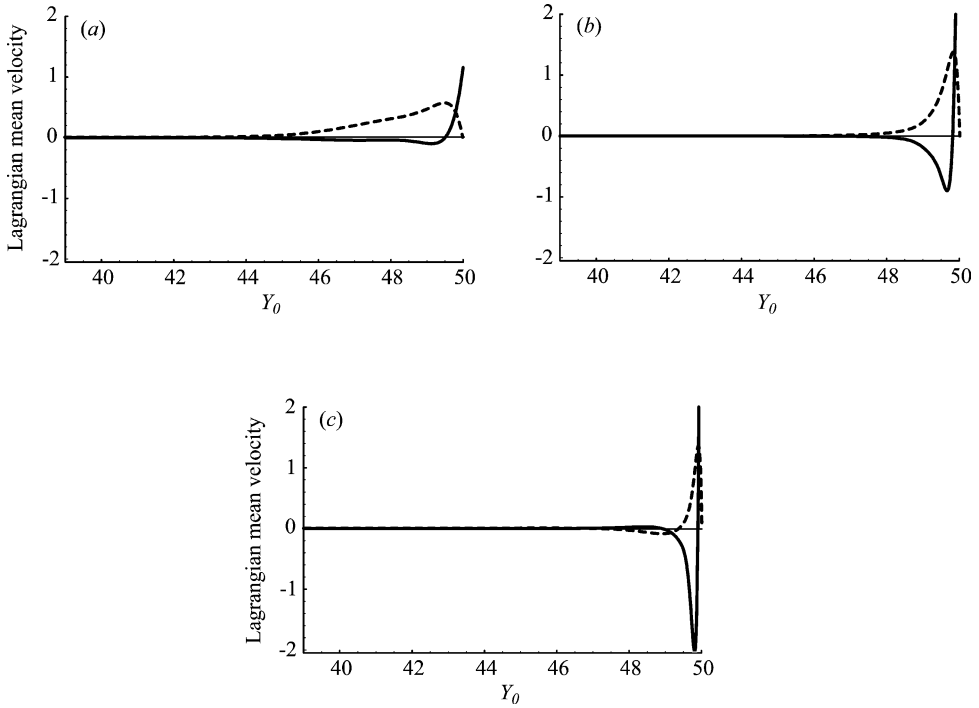

Fig. 7. Time-average of second-order Lagrangian velocities as a function of the initial position Y_0. Solid lines are $\langle u_2^L(t)\rangle$ and dashed lines are $\langle v_2^L(t)\rangle$. Profiles are at $x = 2\pi/3$ and $H = 50$. (a) $\alpha^2 = 2$; (b) $\alpha^2 = 50$; (c) $\alpha^2 = 150$.

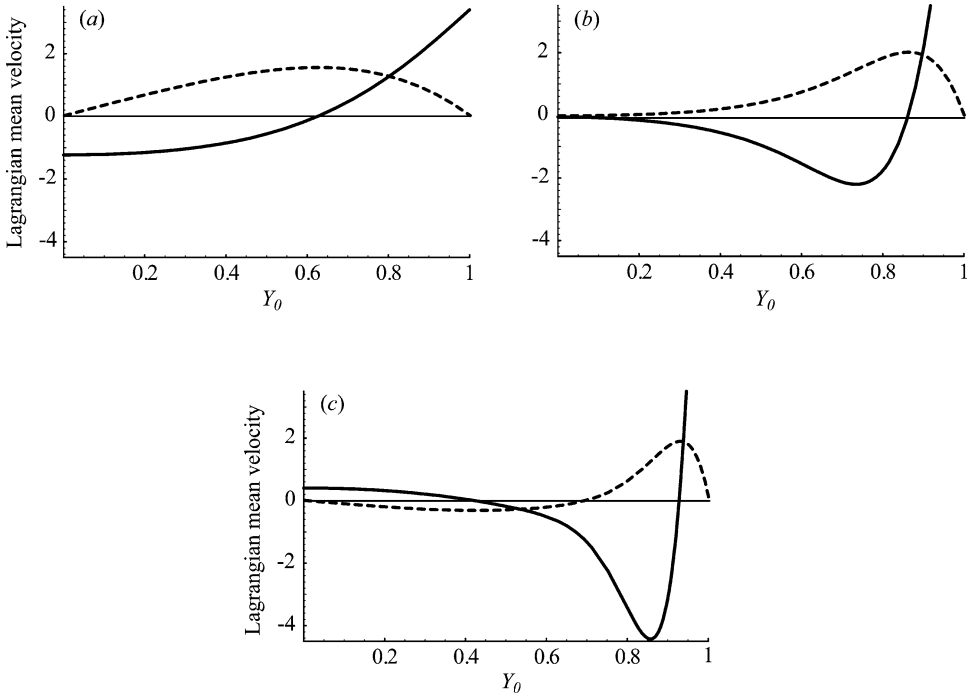

Fig. 8. Time-average of second-order Lagrangian velocities as a function of the initial position Y_0. Solid lines are $\langle u_2^L(t)\rangle$, and dashed lines are $\langle v_2^L(t)\rangle$. Profiles are at $x = 2\pi/3$ and $H = 1$. (a) $\alpha^2 = 10$; (b) $\alpha^2 = 100$; (c) $\alpha^2 = 300$.

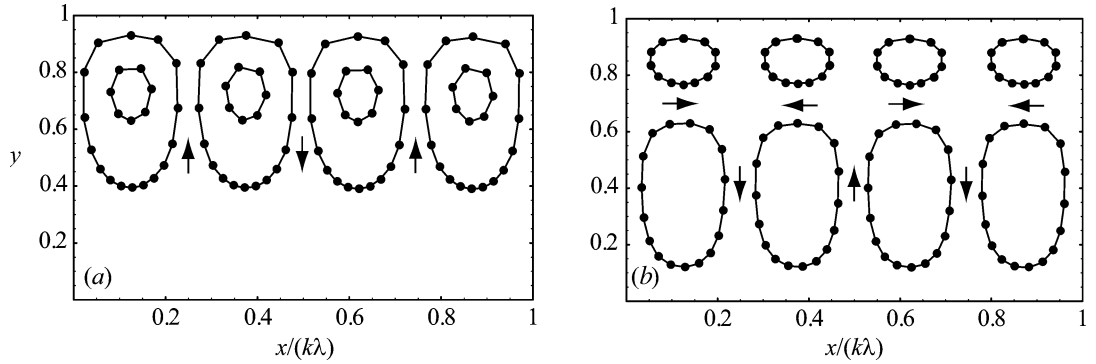

Fig. 9. Poincaré sections illustrating net transport of passive scalars in flow. Dots represent sampled particle positions connected by solid lines. $H = 1$ and (a) $\alpha^2 = 100$; (b) $\alpha^2 = 300$.

To illustrate the mean spatial drift of passive tracers and to determine the characteristics of the mixing, Poincaré sections are created by sampling the particle position at a predetermined frequency. The present flow field is periodic with time period T, and we therefore construct the Poincaré sections as

$$\mathbf{X}_n = \big(X(nT), Y(nT)\big). \tag{27}$$

Fig. 9 shows typical stroboscopically sampled paths for 8 different particles distributed over a wavelength of the vibrating surface. Poincaré sections are obtained for $H = 1$ at α^2 of 100 and 300, illustrating the difference between flow regions 1 and 4 of Fig. 6. All points for a specific particle are furthermore connected by a solid line showing the path of the particle within the Poincaré section. It is obvious that particles follow closed orbits, a result also valid for flows in regions 2 and 3. Poincaré sections of these flows are, however, not shown.

Mixing over the full domain of the channel is obtained for flows generated at an H of order unity or lower. For large values of H there is mixing only in the vicinity of the wall. The importance of advective mixing is enhanced with increasing α^2. Most effective mixing of viscous fluids confined by the vibrating walls is thus obtained for flows of high α^2 and low H, i.e. flows in

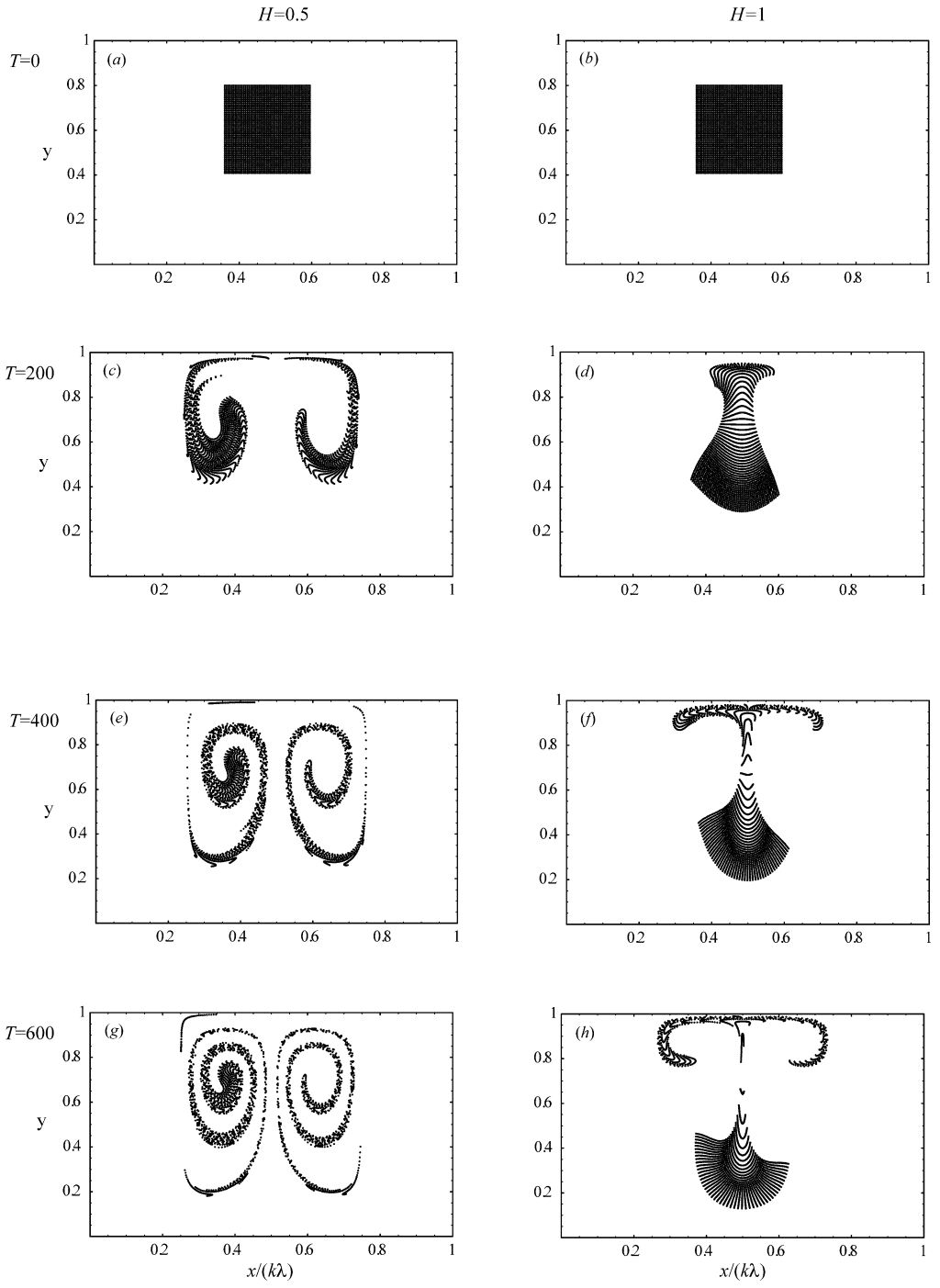

Fig. 10. Advective mixing of 2500 passive scalars evenly distributed in an area confined by $\mathbf{x} = (0.36, 0.6)$ and $\mathbf{y} = (0.4, 0.8)$. $\alpha^2 = 300$. (a) $t = 0$, $H = 0.5$; (b) $t = 0$, $H = 1$; (c) $t = 200T$, $H = 0.5$; (d) $t = 200T$, $H = 1$; (e) $t = 400$, $H = 0.5$; (f) $t = 400T$, $H = 1$; (g) $t = 600T$, $H = 0.5$; (h) $t = 600T$, $H = 1$.

the neighborhood of region 4 in Fig. 6. A vibratory mixer should operate in the vicinity of this flow region in order to be most efficient.

To demonstrate the ability of the steady streaming to mix fluids, 2500 particles are evenly distributed in an area confined by $\mathbf{x} = (0.36, 0.6)$ and $\mathbf{y} = (0.4, 0.8)$. The limits of the box are chosen slightly asymmetrical compared to the cellular flow in

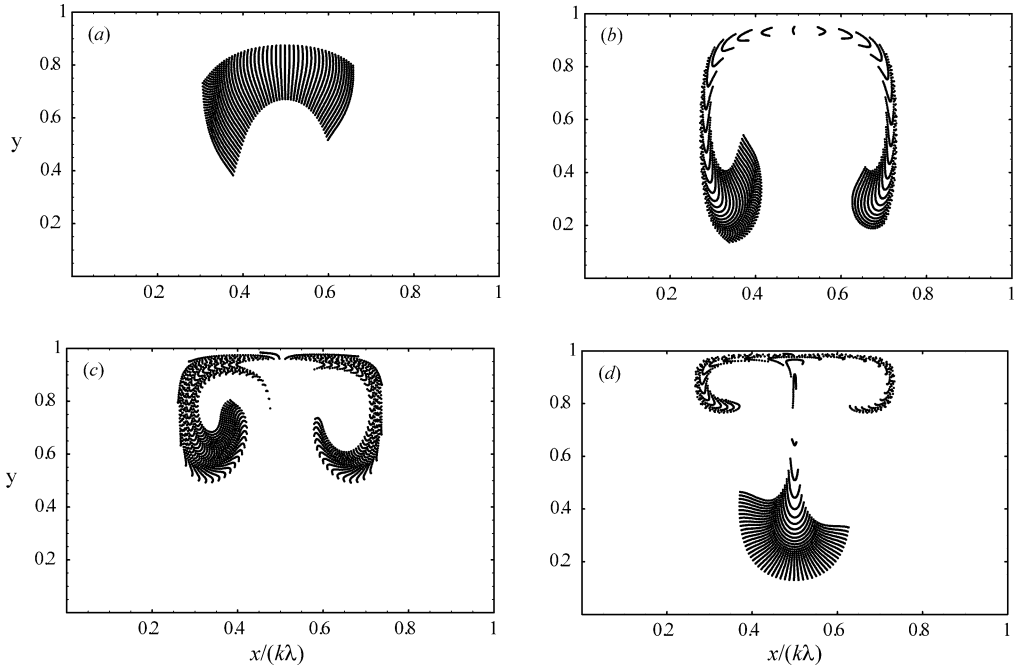

Fig. 11. Advective mixing of 2500 passive scalars evenly distributed in an area confined by $\mathbf{x} = (0.36, 0.6)$ and $\mathbf{y} = (0.4, 0.8)$. $H = 1$. (a) $\alpha^2 = 2$, (b) $\alpha^2 = 10$, (c) $\alpha^2 = 100$, (d) $\alpha^2 = 300$.

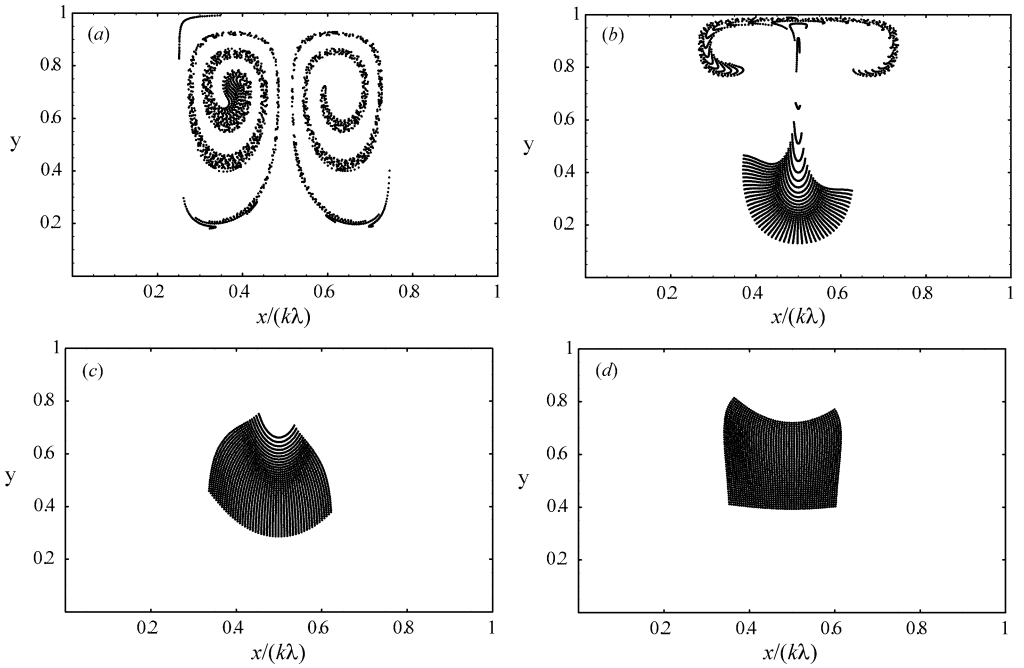

Fig. 12. Advective mixing of 2500 passive scalars evenly distributed in an area confined by $\mathbf{x} = (0.36, 0.6)$ and $\mathbf{y} = (0.4, 0.8)$. $\alpha^2 = 300$ and $T = 600$. (a) $H = 0.5$; (b) $H = 1$; (c) $H = 2$; (d) $H = 4$.

order to better illustrate the deformation of the material region. Fig. 10 describes the advective transport of these particles with time for $H = 0.5$ and $H = 1$, respectively, and $\alpha^2 = 300$. The particles are rapidly spread in the channel and thereby increasing the impact of molecular diffusion; the patterns obtained moreover resembles the corresponding Eulerian flow fields. For both

values of H, the particles are distributed over the full channel half-width; the lower H, however, distributes the particles more rapidly. Showing the particle positions for extremely long times is not justified since the error increases as time proceeds.

Altering α^2 not only impacts the ratio between molecular and advective diffusion, it alters the structure of the streaming flow. In Fig. 11 particle positions are shown at different α^2 for $H = 1$. Both the spreading rate and the particle distribution pattern are affected by the variations in α^2. Generally the particles are better mixed the higher the α^2.

Fig. 12 depicts the positions of the particles at $T = 600$ and $\alpha^2 = 300$ for several values of H. It is clearly seen that mixing is less effective for large values of H.

5. Conclusions

We have addressed the mixing properties of flows generated by solid walls undergoing transverse vibrations in the form of standing waves. The analysis has primarily been motivated by the capability of these flows to enhance mixing in highly viscous fluids. No quantitative measure of mixing has been attempted here and, in this sense, the increases or decreases observed are qualitative.

Analytical expressions of the oscillatory and streaming flow confined in an infinite two-dimensional channel with vibrating walls were used to compute Lagrangian mean velocities and particle paths. Analytical solutions were obtained for the Lagrangian mean velocities by using perturbation methods with the slope of the wall as a perturbation parameter. Particle paths were constructed by numerical integration of the Eulerian flow field.

We first determined the mean Lagrangian velocity for specific particles. A range of dimensionless frequencies α^2 and channel half-widths H were considered. The Lagrangian velocity obtained at a certain initial position qualitatively imitated the Eulerian mean velocity obtained at the same point for flows residing in regions 1, 3 and 4. In region 2, however, there is qualitative difference between the Lagrangian and Eulerian velocities in the vicinity of the wall.

The structure of the mean spatial drift of a passive scalar was determined by the construction of Poincaré sections. Particle paths were found to form closed orbits for the second-order correct calculations described here.

Finally, we demonstrated how the streaming motions in the vibrating channel deformed a region consisting of several passive tracers. The most effective mixing was observed for flows obtained at channel half-widths H of order unity or lower and for sufficiently high values of α^2.

References

[1] F. Carlsson, M. Sen, L. Löfdahl, Steady streaming due to vibrating walls, Phys. Fluids 16 (2004) 1822–1825.
[2] D.P. Telionis, Unsteady Viscous Flows, Springer, New York, 1981.
[3] N. Riley, Steady streaming, Ann. Rev. Fluid Mech. 33 (2001) 43–65.
[4] W.H. Lyne, Unsteady viscous flow over a wavy wall, J. Fluid Mech. 50 (1971) 33–48.
[5] A. Kaneko, H. Honji, Double structures of steady streaming in the oscillatory viscous flow over a wavy wall, J. Fluid Mech. 93 (1978) 727–736.
[6] D. Volfson, J. Vinals, Flow induced by a randomly vibrating boundary, J. Fluid Mech. 432 (2001) 387–408.
[7] M.Y. Jaffrin, A.H. Shapiro, Peristaltic pumping, Ann. Rev. Fluid Mech. 3 (1971) 13–37.
[8] T. Hung, T.B. Brown, Solid-particles motion in two-dimensional peristaltic flow, J. Fluid Mech. 73 (1976) 77–96.
[9] C. Pozrikidis, A study of peristaltic flow, J. Fluid Mech. 180 (1987) 527–551.
[10] M. Li, J.G. Brasseur, Nonsteady peristaltic transport in finite length tubes, J. Fluid Mech. 248 (1993) 129–151.
[11] S. Takabatake, K. Ayukawa, Numerical studies of two-dimensional peristaltic flows, J. Fluid Mech. 122 (1982) 439–465.
[12] S. Takabatake, K. Ayukawa, A. Mori, Peristaltic pumping in circular cylindrical tubes: a numerical study of fluid transport and its efficiency, J. Fluid Mech. 193 (1988) 267–283.
[13] S. Miyazaki, T. Kawai, M. Araragi, A piezoelectric pump driven by a flexural progressive wave, in: Proceedings of the IEEE Micro Electro Mechanical Systems, IEEE, New York, 1991, pp. 283–288.
[14] R.M. Moroney, R.M. White, R.T. Howe, Ultrasonically induced microtransport, in: IEEE Trans., IEEE, New York, 1991, pp. 272–282.
[15] M.C. Sharatchandra, M. Sen, M. Gad-El-Hak, Navier–Stokes simulations of a novel viscous pump, J. Fluids Engrg. 119 (1997) 372–382.
[16] J. Evans, D. Liepmann, A.P. Pisano, Planar laminar mixer, in: The Tenth Annual International Workshop on Micro Electro Mechanical Systems, Proc. IEEE, IEEE, New York, 1997, pp. 96–101.
[17] M. Yi, H.H. Bau, The kinematics of bend-induced mixing in micro-conduits, in: IMECE MicroFluidics Symposium, Orlando, FL, 2000.
[18] A.D. Stroock, S.K.W. Dertinger, A. Ajdari, I. Mezic, H.A. Stone, G.M. Whitesides, Chaotic mixer for microchannels, Science 295 (2002) 647–651.
[19] K.P. Selverov, H.A. Stone, Peristaltically driven channel flows with applications toward micromixing, Phys. Fluids 13 (2001) 1837–1859.
[20] M. Yi, H.H. Bau, H. Hu, Peristaltically induced motion in a closed cavity with two vibrating walls, Phys. Fluids 14, 184–197.